Journal of Materials Chemistry A

PAPER

View Article Online
View Journal | View Issue

Cite this: J. Mater. Chem. A, 2016, 4, 4457

Sulfur-doping achieves efficient oxygen reduction in pyrolyzed zeolitic imidazolate frameworks†

Chao Zhang,[a] Bing An,[a] Ling Yang,[a] Binbin Wu,[a] Wei Shi,[a] Yu-Cheng Wang,[a] La-Sheng Long,[a] Cheng Wang*[a] and Wenbin Lin*[ab]

Received 26th January 2016
Accepted 16th February 2016

DOI: 10.1039/c6ta00768f

www.rsc.org/MaterialsA

We report the first synthesis of sulfurated porous carbon materials with well-defined morphologies and uniform N/S distributions *via* pyrolysis of zeolitic imidazolate frameworks loaded with sulfur-containing molecules. The optimized sulfurated catalyst demonstrates excellent electrocatalytic activity for the oxygen reduction reaction (ORR) in both acid and alkaline media. The sulfurization process under optimized conditions can lower the ORR over-potential by *ca.* 170 mV at 3 mA cm^{-2}, giving a non-precious metal catalyst with an onset ORR potential of 0.90 V (*vs.* RHE, similarly hereinafter)/half-wave potential of 0.78 V in 0.1 M $HClO_4$ and an onset ORR potential of 0.98 V/half-wave potential of 0.88 V in 0.1 M KOH. Furthermore, the S-doped porous carbon materials perform better in the long-term durability test than the non-S-doped samples and standard commercially available Pt/C. We also discuss different sulfuration methods for the ZIF system, morphologies of pyrolyzed samples, and catalytically active sites.

Introduction

Fuel cells are widely considered a promising next-generation green technology to power vehicles and other devices.[1–3] The search for an economically viable noble-metal-free catalyst for the cathodic oxygen reduction reaction (ORR) is one of the key steps towards the large scale implementation of fuel cell technology.[4–6] Current commercial catalysts, which are based on noble metals (*e.g.*, Pt/C), not only lead to high catalyst costs, but also suffer from low poison resistance (*e.g.*, by methanol) and poor durability.[7–12] Significant progress has been made in alternative non-precious metal catalysts (NPMCs) based on transition metal–nitrogen–carbon (TM–N–C, TM = Mn, Fe, Co, Ni, *etc.*) systems.[13–19] These catalysts exhibit high activity for the ORR when operating under basic conditions (0.1 M KOH), even surpassing the performance of Pt/C. Furthermore, metal-free, hetero-atom-doped carbon materials were also discovered to give high ORR activity in alkaline media,[20,21] which are applicable to metal–air fuel cells. However, commercial cells that use hydrogen as the fuel operate under acidic conditions due to the Nafion membrane, which functions as a proton conductor while preventing electron conduction and fuel/O_2 crossover. The corresponding membrane for hydroxide conduction under basic conditions has not yet met requirements for fuel cells.[22,23] Thus, for hydrogen fuel cells, an NPMC that can operate under acidic conditions is more desirable because it is readily adaptable to the current technology.

Reports of TM–N–C catalysts under acidic conditions are much fewer, and their over-potentials in the ORR are much higher than that of Pt/C. Among the efforts to prepare NPMCs in acidic media, Sun *et al.* reported in 2015 that the use of $Fe(SCN)_3$ instead of $FeCl_3$ in the pyrolytic preparation of Fe/N/C catalysts can significantly reduce the ORR over-potential. They obtained an S-doped-Fe/N/C catalyst with a half-wave potential of 0.836 V *vs.* RHE in 0.1 M H_2SO_4, the highest (or lowest over-potential) among all reported NPMC under acidic conditions.[24] S-doped graphene also showed improved ORR activity.[25] In similar cases, studies on S/N co-doped graphene and porous carbon also revealed a beneficial change in the electronic structure for the ORR.[13,26–28] Other examples of S-doped NPMCs include thiophene/thiourea-doped carbon materials and the carbonization of S,N-containing precursors,[29–32] although most of the tests were conducted under basic conditions.

Here, we explore the pyrolysis of metal–organic frameworks (MOFs) as a strategy to introduce metal and hetero-atoms into a conductive carbon matrix. The different element components are evenly mixed at a molecular level in a solid porous MOF precursor, which results in homogeneously distributed active centers in highly porous carbon matrices upon pyrolysis, a desirable feature for electrocatalysis. The metal components are incorporated into the MOF precursor as metal nodes, whereas hetero-atoms such as nitrogen can be introduced

[a]Collaborative Innovation Center of Chemistry for Energy Materials, State Key Laboratory of Physical Chemistry of Solid Surfaces, Department of Chemistry, College of Chemistry and Chemical Engineering, Xiamen University, Xiamen 361005, P.R. China. E-mail: wangchengxmu@xmu.edu.cn

[b]Department of Chemistry, University of Chicago, 929 E 57th Street, Chicago, IL 60637, USA. E-mail: wenbinlin@uchicago.edu

† Electronic supplementary information (ESI) available. See DOI: 10.1039/c6ta00768f

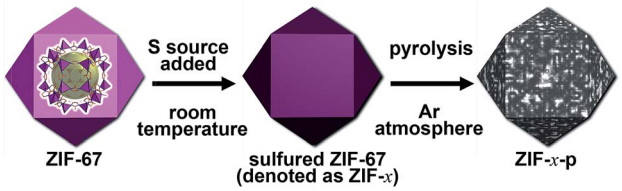

Scheme 1 The preparation of ZIF-*x*-p for ORR electrocatalysis.

through N-containing ligands. In addition, other elements can be easily brought into the MOF cavity or integrated through post-synthetic modification of the MOFs.[33,34] We have previously used post-synthetic sulfurization of MOFs to obtain highly porous S-containing materials.[35] We thus proposed to use MOF sulfurization and pyrolysis as a versatile strategy to discover highly active S-doped ORR catalysts (Scheme 1).

There are several reports on the generation of NPMCs from the pyrolysis of zeolitic imidazolate frameworks (ZIFs), a special category of MOFs constructed from Co^{2+}, Zn^{2+}, or Fe^{2+} and nitrogen-containing imidazolate ligands.[33,36–43] A few of these have exhibited ORR activity under acidic conditions.[33,39–41] We chose the Co^{2+}-based **ZIF-67** as the precursor in the sulfurization/pyrolysis strategy we used to improve the ORR activity under acidic conditions.[44] We found that under optimized conditions the sulfurization process can lower the ORR overpotential by *ca.* 170 mV at 3 mA cm^{-2}, giving an NPMC with an onset ORR potential of 0.88 V and a half-wave potential of 0.78 V in 0.1 M $HClO_4$. The diffusion-limited current of 5.8 mA cm^{-2} (at 0.4 V) is also comparable to that of the most active catalysts reported in the literature. This catalyst also exhibits superb ORR activity in alkaline media, with an onset ORR potential of 0.98 V and a half-wave potential of 0.88 V in 0.1 M KOH and a diffusion-limited current of 5.4 mA cm^{-2} at 0.4 V, surpassing the performance of commercial Pt/C (Fig. 1).[34,38,40–45]

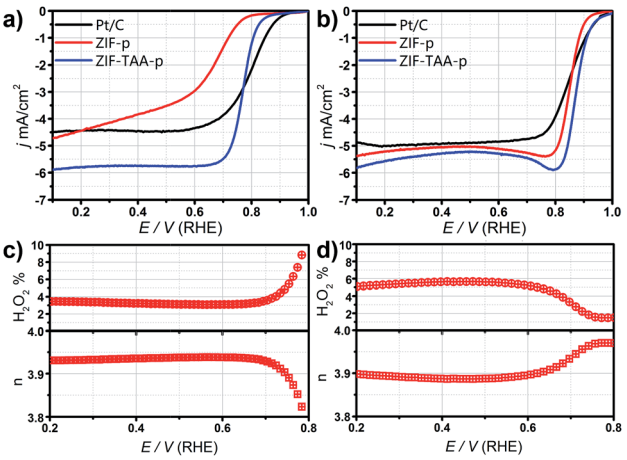

Fig. 1 RRDE voltammograms of optimized ZIF-TAA-p (stirred with TAA for 1 h at room temperature and pyrolyzed at 700 °C for 10 min), ZIF-p, and Pt/C (a) in an O_2-saturated 0.1 M $HClO_4$, (b) in an O_2-saturated 0.1 M KOH, and ((c) and (d)) their respective H_2O_2 yields and electron transfer numbers at a rotation rate of 1600 rpm.

Experimental section

Materials and methods

All chemicals were obtained from commercial sources and used without further purification: 2-methylimidazole (99%) was purchased from InnoChem Science & Technology (Beijing, China); zinc nitrate hexahydrate (99%) and cobalt nitrate hexahydrate (99%) were purchased from Sinopharm Chemical Reagent Co., Ltd. Methanol (AR) and ethanol (AR) were purchased from Sinopharm Chemical Reagent Co., Ltd. Distilled water with the specific resistance of 18.2 MΩ cm was obtained by Direct-Q 3UV.

Synthetic procedures

Preparation of ZIF-67 nanocrystals. Synthesis of **ZIF-67** was based on the procedure in the literature.[34] Typically, 0.45 g of $Co(NO_3)_2 \cdot 6H_2O$ was dissolved in 3 mL of pure water; then 5.5 g of 2-methylimidazole in 20 mL of water was added with vigorous stirring. The reaction proceeded for 6 hours at room temperature. The resulting purple precipitates were collected by centrifugation, washed with methanol in sequence 3 times, and finally dried in a vacuum box at 50 °C overnight.

Preparation of ZIF-TAA, ZIF-TU, ZIF-SCN, and ZIF-TP. 0.3 g of the dried ZIF was transferred into 10 mL of a 0.1 M **TAA/TU/SCN/TP** solution of ethylene glycol. After vigorously stirring for a controlled reaction time, the product was separated by centrifugation, washed thoroughly with methanol 3 times, and dried at 50 °C overnight. This preparation produces yields of greater than 90%.

Preparation of ZIF-S. The synthesis procedure of **ZIF-S** is similar to that of **ZIF-TAA**, except that ethanol was used as the solvent, producing a yield of greater than 90%.

Preparation of ZIF-p and ZIF-*x*-p (*x* indicates the sulfur sources). 0.3 g of the sample was heated to a desired temperature at a heating rate of 5 °C min^{-1} and carbonized at a controlled temperature for a controlled amount of time under Ar flow (50–80 mL min^{-1}), then cooled to room temperature naturally to obtain **ZIF-p** and **ZIF-*x*-p**. This preparation yields 35–50% for **ZIF-p** and 40–60% for sulfurated samples.

Electrochemical measurements

Evaluation of the catalytic performance in the ORR. The ORR performance was tested in O_2-saturated 0.1 M $HClO_4$ or 0.1 M KOH at room temperature on a rotating-disk electrode (RDE) or a rotating Pt-ring-disk electrode (RRDE) system (Pine Inc, GC, d = 5 mm) with a CH Instrument-660e electrochemical workstation or Pine WaveDrive 20 bipotentiostat. The rotating rate was 1600 rpm. A platinum wire and Ag/AgCl (3.5 M KCl) were used as the counter and reference electrodes, respectively. The reference electrode was calibrated to a reversible hydrogen electrode (Fig. S20†) (potential was converted to potential *vs.* RHE according to $E_{\text{potential vs. RHE}} = E_{\text{potential vs. Ag/AgCl}} + 0.2046\ \text{V} + 0.0592\text{pH}$). To prepare the catalyst ink, 5 mg of the pyrolyzed samples was ultrasonically dispersed in a mixture of ethanol (0.48 mL) and 5% Nafion (0.02 mL) for 1 hour. 10 μL of the resulting ink was pipetted onto the GC disk electrode. The

loading of the Pt/C (20 wt%) catalyst was 0.5 mg cm^{-2}. Polarization curves were recorded by potential cycling between 0.1 and 1.0 V *vs.* RHE at 10 mV s^{-1}. The solution ohmic drop (that is, *iR* drop) was compensated. To determine H_2O_2 yield and the number of electrons transferred (n), the ring electrode was held at 1.35 V *vs.* RHE to oxidize H_2O_2 diffusing from the disk electrode. The H_2O_2 yield and n can be calculated with the following equations, where N is the collection efficiency (26%) and I_{disk} and I_{ring} are the voltammetric currents at the disk and ring electrodes, respectively:

$$H_2O_2\% = \frac{200I_{ring}/N}{I_{ring}/N + I_{disk}} \quad (1)$$

$$n = \frac{4I_{disk}}{I_{ring}/N + I_{disk}} \quad (2)$$

Resistance measurements. All samples were pressed into small tablets and carefully painted on each side with conductive adhesive with Ag wires. The areas of conductive adhesive and thicknesses of tablets were recorded and denoted as S and L, respectively. The current (I) changes were recorded alone with the voltage (U, −1 V to +1 V) on a Keithley 2400 Source Meter, and the electrical resistance (R) could be obtained by Ohm's law. The electrical conductance (ρ) was obtained by measuring the electrical resistance, the area of conductive adhesive, and the thickness of the tablet.

$$R = U/I \quad (3)$$

$$\rho = RS/L \quad (4)$$

Results and discussion

We begin catalyst preparation by stirring 0.3 g of **ZIF-67** nanocrystals with 10 mL of a 0.1 M solution of thioacetamide (**TAA**) at room temperature (25–30 °C) for 1 hour to afford **TAA**-loaded ZIFs (denoted as **ZIF-TAA**).[46] The powder X-ray diffraction (XRD) pattern of **ZIF-TAA** was the same as that of the original **ZIF-67** (Fig. 2a), indicating that the small amount of **TAA** is either absorbed inside the ZIF cavity in a molecular form or exists as amorphous CoS_x (S^{2-} anions from hydrolyzed **TAA** react with the Co^{2+} from the **ZIF-67**, resulting in the amorphous CoS_x).[46] The color of **ZIF-TAA** became darker than **ZIF-67**, supporting the formation of CoS_x. Thermal Gravimetric Analyses (TGA) of **ZIF-67** and **ZIF-TAA** in air are also consistent with CoS_x formation, with increased residue weights (Fig. S1†). These **TAA**-loaded samples were then pyrolyzed at 700 °C for 10 minutes under Ar to give black powders (denoted as **ZIF-TAA-p**, where p denotes pyrolysis). Examination of the **ZIF-TAA-p** sample under a Transmission Electron Microscope (TEM) showed that **ZIF-67**, **ZIF-TTA**, and **ZIF-TTA-p** were of similar particle sizes (50–200 nm; see Fig. 3), suggesting single-particle-to-single-particle transformation during the sulfurization/pyrolysis processes. The **ZIF-TTA-p** also contained a number of smaller dots (5–20 nm) within the particle (Fig. S2†), which were identified as

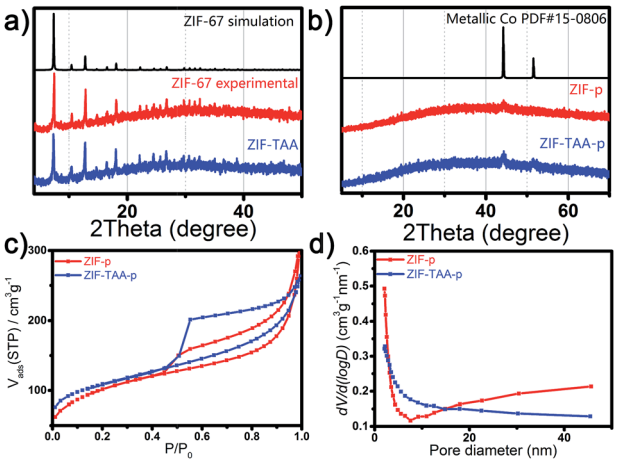

Fig. 2 Powder XRD patterns of samples (a) before pyrolyzed and after pyrolyzed; (b) N_2 sorption isotherms of **ZIF-p** and **ZIF-TAA-p** (c) and (d) corresponding pore size distribution.

cobalt metal nanoparticles (Co-NPs) based on the PXRD patterns of the samples (Fig. 2b). The resultant **ZIF-TTA-p** contains 29.96 wt% of Co, 1.51 wt% of S, 9.91 wt% of N and 39.76 wt% of C, as determined by a combination of ICP-MS and elemental analysis (Table S3†). These Co-NPs were wrapped with carbon shells and the Co-NPs could even be observed after dilute acid washing (Fig. S3†). However, ICP-MS reveals that 18.63 wt% and 32.70 wt% of Co species in **ZIF-TAA-p** dissolved after treating with 0.1 M $HClO_4$ for 2 and 24 hours, respectively, which can account for declining ORR activities of **ZIF-TAA-p** in acid media as discussed below. These Co-NPs almost completely disappear by hydrothermal etching with 10 M HCl at 180 °C for 24 hours (Fig. S4†).

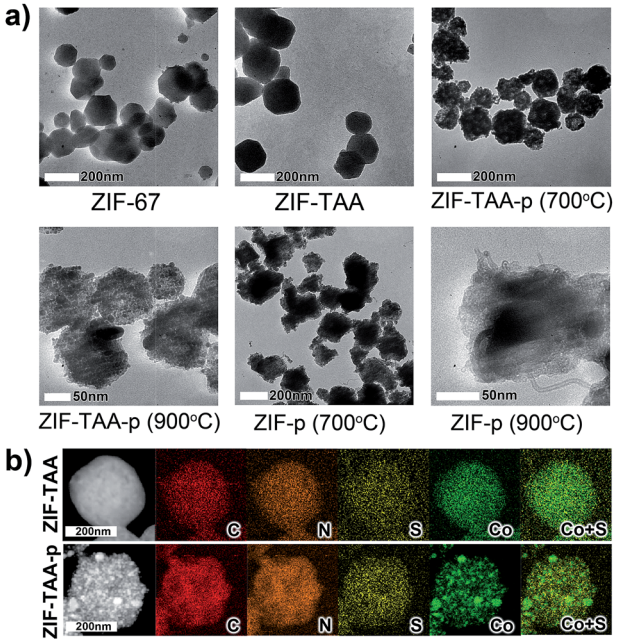

Fig. 3 (a) TEM images of different samples. (b) EDX mapping of C, N, S, and Co for **ZIF-TAA** and **ZIF-TAA-p**.

The catalysts were further sulfurated by stirring 0.3 g of **ZIF-67** nanocrystals with 10 mL of a 0.1 M solution of other sulfurization agents (**TU:** thiourea, **SCN:** NH_4SCN, **S:** sublimed sulfur, and **TP:** thiophene) at room temperature for 1 hour followed by pyrolysis (the pyrolyzed samples are denoted as **ZIF-*x*-p**, where *x* is the sulfurization agent).[46] The ORR activity tests of these samples were conducted in an O_2-saturated 0.1 M $HClO_4$ solution using a rotating-disk electrode (RDE). Nafion was mixed with the samples to prepare the electrode for the test. As shown in Fig. 4a, **ZIF-TAA-p** has a better ORR performance than other sulfurized samples and non-sulfurized **ZIF-p**. The ORR activity of **ZIF-TAA-p** was further optimized by adjusting the stirring duration (Fig. 4b), the pyrolysis temperature (Fig. 4c), and the pyrolysis duration (Fig. 4d) to obtain the highest ORR activity, which resulted when **ZIF-TTA-p** was stirred with **TAA** for 1 hour at room temperature and then subjected to pyrolysis at 700 °C for 10 minutes. The observed half-wave potential of 0.78 V *vs.* RHE for **ZIF-TAA-p** under acidic conditions is comparable to that of the best ZIF-derived Fe–N–C NPMCs.[33] It is worth noting that Fe–N–C NPMCs have usually shown better performances than Co–N–C NPMCs.[39,47,48] This half-wave potential is also 170 mV higher than that of the sample without sulfurization that was pyrolyzed under the same conditions (**ZIF-p**), thus highlighting the beneficial effect of S-doping. Consistent with the RDE, the CV curve for **ZIF-TAA-p** displays a characteristic ORR peak centered at about 0.71 V (Fig. S5†). The ORR activities of the catalysts were also tested in alkaline media (0.1 M KOH), giving a half-wave potential of 0.88 V (Fig. 1b) for **ZIF-TAA-p**. All these ORR measurements can be easily reproduced with different batches of catalysts prepared following the same procedure. The numbers of electrons transferred (*n*), calculated from the H_2O_2 percent yields in the rotating ring disc electrode (RRDE, Fig. S6†) measurements, are very close to 4 (3.80 to 3.94 for acidic media and 3.89 to 3.97 in the basic media), confirming the reduction of oxygen to water as the main reaction (Fig. 1c and d).

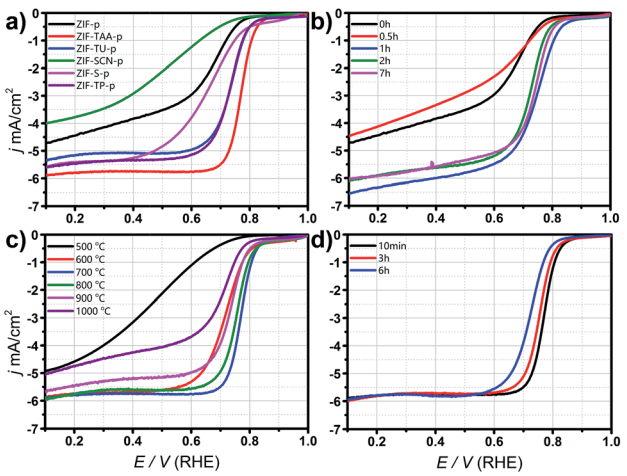

Fig. 4 RDE voltammograms of (a) optimized ZIF-TAA-p and ZIF-*x*-p at (b) different stirring durations, (c) different pyrolysis temperatures (pyrolyzed for 10 minutes), and (d) different pyrolysis durations (at 700 °C). All measurements were conducted in O_2-saturated 0.1 M $HClO_4$ at a rotation rate of 1600 rpm.

The stability of **ZIF-TAA-p** under acidic conditions was also much better than that of Pt/C. After a 24 hour electrolysis test, its catalytic current dropped to 65% of its original value, while, in comparison, the catalytic current of Pt/C dropped to about 11% after only 3 hours of electrolysis (Fig. S7a†). The stability of **ZIF-TAA-p** is also much better than other reported non-doped **ZIF-67**-derived catalysts tested under the same conditions.[47] The decline of long-term ORR activity may be related to the dissolution of active Co-species in the acid media as mentioned above. Moreover, we also observed that after soaking for 5 hours in 0.1 M $HClO_4$, the ORR activity of **ZIF-TAA-p** declined (Fig. S7b†). Since no Co species were dissolved in alkaline media (less than 0.01 wt% of Co dissolution in 0.1 M KOH after 24 hours based on ICP results), **ZIF-TAA-p** has a much better stability in ORR performance in alkaline media: less than 5% of current decline was observed after the electrolysis test of 24 hours (Fig. S8†). Moreover, the ORR activity of **ZIF-TAA-p** remains the same after 5000 cycles of LSV in alkaline media (Fig. S9†). Like other NPMCs, **ZIF-TAA-p** is also tolerant to methanol in contrast to Pt/C (Fig. S10†), a property that is crucial for methanol fuel cells. These results indicate that Co-species play important roles in ORR (especially in acid media). The doping of sulfur not only enhances the catalytic activities of the ZIF-derived **ZIF-TAA-p** but also improves its stability.

Encouraged by the superb ORR activity of S-doped, pyrolyzed MOFs, we proceeded to investigate the nature and influence of S-doping. The ORR activity of a catalyst can be related to several factors: (1) the intrinsic activity or chemical nature of the active sites; (2) the electrochemically accessible surface area of the catalyst; (3) the electron and ion conductivity of the Nafion/catalyst hybrid; (4) the rate of oxygen diffusion into the active centers. We systematically examined the effect of S-doping on some of these factors.

The chemical nature of the active sites

We began the investigation by examining the sulfur element distribution in **ZIF-TAA-p** with Energy Dispersive X-ray (EDX) mapping (Fig. 3b). While the Co atoms were segregated into cobalt nanoparticles, the N and S were uniformly dispersed throughout the carbon matrix, suggesting the formation of S/N co-doped carbon together with the encapsulated Co-NPs.[34] We believe the Co-NP is an active component of the ORR catalyst. This notion is consistent with an acid etching experiment: the sample hydrothermally treated in 10 M HCl at 180 °C for 24 hours[41] exhibited dissolution of parts of the encapsulated Co-NPs, together with reduced ORR activity (Fig. S4 and S11a†). In addition, a sample without Co (prepared from the Zn-containing **ZIF-8**, an isostructure to **ZIF-67**, under the same sulfurization and pyrolysis conditions) exhibited poor ORR activity (Fig. S11b†).

The element mapping of Co cannot rule out the possibility of coordinated CoN_x/CoS_x as other types of Co species dispersed in the carbon matrix. The involvement of such species in the ORR was supported by a SCN^- poisoning experiment, in which the addition of 12 mM KSCN, a coordination poison of TM ion centers,[17] quenched 10% of the cathodic current (Fig. S12†). We

thus concluded that both the metallic Co-NPs and CoN_x/CoS_x species likely contribute to the ORR activity.[49,50]

The elemental analysis showed that, compared to **ZIF-p**, the **ZIF-TAA-p** contains slightly more nitrogen (9.91 wt% for **ZIF-TAA-p** *vs.* 6.70 wt% for **ZIF-p**). Both **ZIF-p** and **ZIF-TAA-p** contain metallic Co-NPs according to the intensities of the PXRD patterns (Fig. 2b). The TEM images also reveal an important difference in morphology between **ZIF-TAA-p** and **ZIF-p**: **ZIF-p** begins to form carbon nanotubes at 700 °C (Fig. 3a and S13†) while **ZIF-TAA-p** keeps the original particle size of the ZIF even when increasing the pyrolysis temperature (up to 900 °C, Fig. 3a and S2†) or extending the pyrolysis duration (up to 6 hours, Fig. S14†). Such structural differences not only change the mass transfer patterns within the catalysts, but also indicate differences between the chemical natures of the carbon matrices.

X-ray photoelectron spectroscopy (XPS) was employed to further investigate the chemical nature of **ZIF-*x*-p**. The Co $2p_{3/2}$ peaks (Fig. S5 and S15†) revealed both metallic Co (778.3 eV) and divalent Co(II) (780.4 eV) in **ZIF-p** and **ZIF-TAA-p**.[41] **ZIF-TAA-p** contains more metallic Co than **ZIF-p** (19.36% in **ZIF-TAA-p** *vs.* 11.05% in **ZIF-p**, Fig. 5, Table S4†), which is consistent with the PXRD patterns (Fig. 2b). The Co(II) species may come from CoN_x and CoS_x. The peaks of the N 1s region on the spectra could all be fitted with two components with peaks at 398.7 eV and 400.1 eV, corresponding to pyridinic- and pyrrolic-N, respectively (Fig. S16†).[42] The percentages of pyridinic-N with respect to total N in the sulfur-doped samples were all higher than that in **ZIF-p** (37.64% in **ZIF-p** *vs.* 53.26% in **ZIF-TAA-p**, Table S5†). The sulfur-doping thus not only increases the amount of nitrogen in the pyrolyzed samples as shown by elemental analysis (Table S3†), but also increases the percentage of pyridinic-N. The pyridinic-N is believed to help the ORR activites.[51–53] All the S 2p peaks in XPS can be fitted with three different sulfur species: Co–S_n–Co at 162.0 eV;[54] C–S_n–C at 164.0 eV,[26] and –SO_n– at 168.8 eV.[26] High percentages of –SO_n– with respect to total S were observed in **ZIF-SCN-p** (73.15%, Table S6†) and **ZIF-S-p** (49.25%), correlated with their poor conductivities and reduced ORR performances. In comparison, **ZIF-TAA-p** had the majority of sulfur as Co–S_n–Co and C–S_n–C, and exhibited the highest ORR activity (Fig. 5).[24,26]

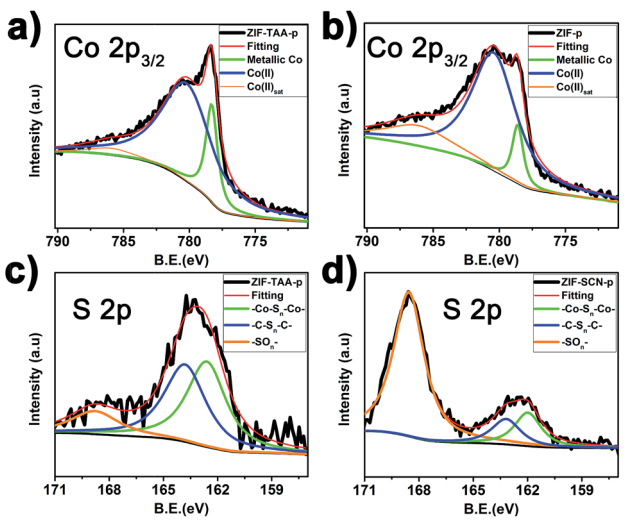

Fig. 5 XPS spectra of Co $2p_{3/2}$ for (a) **ZIF-TAA-p** and (b) **ZIF-p**; XPS spectra of S 2p for (c) **ZIF-TAA-p** and (d) **ZIF-SCN-p**.

Electrochemically accessible surface area

We first measured the geometric surface areas of S-doped **ZIF-TAA-p** and non-doped **ZIF-p** by N_2 adsorption at 77 K (Fig. 2c). Both **ZIF-p** and **ZIF-TAA-p** exhibit type IV adsorption curves with the characteristic hysteresis loop of mesopores. The surface areas of **ZIF-p** and **ZIF-TAA-p** are 368.10 $m^2\ g^{-1}$ and 382.79 $m^2\ g^{-1}$ respectively. The S-doping thus does not change BET surface areas of the pyrolyzed ZIFs. On the other hand, the S-doping does have a small effect on the pore-size distribution (Fig. 2d), which can affect mass transfer in ORR.[55,56] We also evaluated the electrochemically accessible surface area by measuring the specific double-layer capacitance (C_{DL}) of **ZIF-p** and **ZIF-TAA-p** in N_2-saturated 0.1 M $HClO_4$. As demonstrated in Fig. S18,† in a potential window without faradaic processes (0.95–1.05 V), we can obtain the specific capacitance values from the scan rate dependent CV runs. The determined value of 55.0 mF g^{-1} for **ZIF-TAA-p**, as compared to 19.2 mF g^{-1} for **ZIF-p**, indicates that the S-doping does increase electrochemically accessible surface area by three times.

Electron conductivity

The electric conductivities of the catalysts were measured by a two-electrode probe method on catalyst tablets (Fig. 6a and S19 and Table S7†), which showed that both **ZIF-TAA-p** and **ZIF-p** are very conductive carbon matrices. We also observed a relationship between electric conductivity and the catalytic activity of the S-doped catalysts. As mentioned earlier, the samples made with different sulfurization agents but the same pyrolysis procedure showed distinctively different ORR activities (Fig. 4a). **ZIF-TAA-p**, **ZIF-TU-p**, and **ZIF-TP-p** are all relatively active ORR catalysts (with a half-wave potential of >0.7 V *vs.* RHE under acidic conditions), and all of them possess relatively small resistances. In contrast, **ZIF-SCN-p** has a resistance 1–2 orders of magnitude larger than the previous three samples, and its ORR performance is only moderate (with a half-wave potential of *ca.* 0.55 V). For **ZIF-S-p**, which has a resistance larger by another order of magnitude, its ORR activity becomes even worse than that of **ZIF-p**. The electric conductivities of these catalysts were related to their chemical compositions (Fig. 6b):

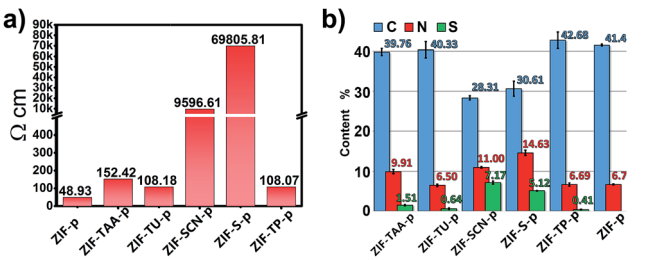

Fig. 6 (a) Resistivity data of **ZIF-*x*-p**; (b) comparison of C, N, and S contents in **ZIF-*x*-p**.

a moderate N + S content is beneficial to ORR activity, but a very high S content (especially the $-SO_n-$ species) and low C content are correlated with poor conductivity and poor ORR activity. As a result, there is a balance between the enhancement of activity induced by S-doping and the drop in conductivity. Such delicate relationships explain why the choice of sulfurization agent, stirring duration, and the pyrolysis temperature and duration can all affect the ORR activity.

Conclusions

In summary, we have demonstrated that the doping of S into an ORR non-precious metal catalyst precursor, **ZIF-67**, can lead to greatly enhanced ORR activity in both acid and alkaline media. The obtained catalyst has a uniform N/S co-doped conductive carbon matrix, together with encapsulated Co nanoparticles and possible CoN_x/CoS_x species. The proper S-doping prevents the formation of carbon nanotubes in the pyrolysis step and retains a large electrochemically accessible surface area. We expect that this S-doping method could be extended to other similar systems and holds great promise as an economically viable substitute for Pt/C in the development of advanced electrode materials.

Acknowledgements

We thank the National Natural Science Foundation of P.R. China (21471126), the National Thousand Talents Program of P.R. China, and the 985 Program of Chemistry and Chemical Engineering disciplines of Xiamen University for support with funding. We thank Ms Ruiyun Huang for her administrative help and Prof. Zhiyou Zhou for his insightful discussion.

Notes and references

1 B. Dunn, H. Kamath and J.-M. Tarascon, *Science*, 2011, **334**, 928–935.
2 J. B. Goodenough, *Acc. Chem. Res.*, 2013, **46**, 1053–1061.
3 P. G. Bruce, S. A. Freunberger, L. J. Hardwick and J.-M. Tarascon, *Nat. Mater.*, 2012, **11**, 172.
4 Y. Nie, L. Li and Z. Wei, *Chem. Soc. Rev.*, 2015, **44**, 2168–2201.
5 W. Yu, M. D. Porosoff and J. G. Chen, *Chem. Rev.*, 2012, **112**, 5780–5817.
6 N. M. Marković and P. N. Ross Jr, *Surf. Sci. Rep.*, 2002, **45**, 117–229.
7 Y. Bing, H. Liu, L. Zhang, D. Ghosh and J. Zhang, *Chem. Soc. Rev.*, 2010, **39**, 2184–2202.
8 Z. Chen, D. Higgins, A. Yu, L. Zhang and J. Zhang, *Energy Environ. Sci.*, 2011, **4**, 3167–3192.
9 X. Ma, H. Meng, M. Cai and P. K. Shen, *J. Am. Chem. Soc.*, 2012, **134**, 1954–1957.
10 Y. Tan, C. Xu, G. Chen, X. Fang, N. Zheng and Q. Xie, *Adv. Funct. Mater.*, 2012, **22**, 4584–4591.
11 S.-I. Choi, S. Xie, M. Shao, J. H. Odell, N. Lu, H.-C. Peng, L. Protsailo, S. Guerrero, J. Park, X. Xia, J. Wang, M. J. Kim and Y. Xia, *Nano Lett.*, 2013, **13**, 3420–3425.
12 S. Xie, S.-I. Choi, N. Lu, L. T. Roling, J. A. Herron, L. Zhang, J. Park, J. Wang, M. J. Kim, Z. Xie, M. Mavrikakis and Y. Xia, *Nano Lett.*, 2014, **14**, 3570–3576.
13 S. Yuan, J.-L. Shui, L. Grabstanowicz, C. Chen, S. Commet, B. Reprogle, T. Xu, L. Yu and D.-J. Liu, *Angew. Chem.*, 2013, **125**, 8507–8511.
14 G. Wu, K. L. More, C. M. Johnston and P. Zelenay, *Science*, 2011, **332**, 443–447.
15 Z. Li, G. Li, L. Jiang, J. Li, G. Sun, C. Xia and F. Li, *Angew. Chem., Int. Ed.*, 2015, **54**, 1494–1498.
16 W. Niu, L. Li, X. Liu, N. Wang, J. Liu, W. Zhou, Z. Tang and S. Chen, *J. Am. Chem. Soc.*, 2015, **137**, 5555–5562.
17 Q. Wang, Z.-Y. Zhou, Y.-J. Lai, Y. You, J.-G. Liu, X.-L. Wu, E. Terefe, C. Chen, L. Song, M. Rauf, N. Tian and S.-G. Sun, *J. Am. Chem. Soc.*, 2014, **136**, 10882–10885.
18 M. Jahan, Q. Bao and K. P. Loh, *J. Am. Chem. Soc.*, 2012, **134**, 6707–6713.
19 H. T. Chung, J. H. Won and P. Zelenay, *Nat. Commun.*, 2013, **4**, 1922.
20 X. Sun, P. Song, Y. Zhang, C. Liu, W. Xu and W. Xing, *Sci. Rep.*, 2013, **3**, 2505.
21 J. Zhang, Z. Zhao, Z. Xia and L. Dai, *Nat. Nanotechnol.*, 2015, **10**, 444–452.
22 O. I. Deavin, S. Murphy, A. L. Ong, S. D. Poynton, R. Zeng, H. Herman and J. R. Varcoe, *Energy Environ. Sci.*, 2012, **5**, 8584–8597.
23 M. A. Hickner, A. M. Herring and E. B. Coughlin, *J. Polym. Sci., Part B: Polym. Phys.*, 2013, **51**, 1727–1735.
24 Y.-C. Wang, Y.-J. Lai, L. Song, Z.-Y. Zhou, J.-G. Liu, Q. Wang, X.-D. Yang, C. Chen, W. Shi, Y.-P. Zheng, M. Rauf and S.-G. Sun, *Angew. Chem., Int. Ed.*, 2015, **54**, 9907–9910.
25 Z. Ma, S. Dou, A. Shen, L. Tao, L. Dai and S. Wang, *Angew. Chem., Int. Ed.*, 2015, **54**, 1888–1892.
26 Y. Su, Y. Zhang, X. Zhuang, S. Li, D. Wu, F. Zhang and X. Feng, *Carbon*, 2013, **62**, 296–301.
27 J. Liang, Y. Jiao, M. Jaroniec and S. Z. Qiao, *Angew. Chem., Int. Ed.*, 2012, **51**, 11496–11500.
28 X. Wang, J. Wang, D. Wang, S. Dou, Z. Ma, J. Wu, L. Tao, A. Shen, C. Ouyang, Q. Liu and S. Wang, *Chem. Commun.*, 2014, **50**, 4839–4842.
29 J. Xu, G. Dong, C. Jin, M. Huang and L. Guan, *ChemSusChem*, 2013, **6**, 493–499.
30 G. Zhuang, J. Bai, X. Tao, J. Luo, X. Wang, Y. Gao, X. Zhong, X. Li and J. Wang, *J. Mater. Chem. A*, 2015, **3**, 20244–20253.
31 W. Yang, X. Yue, X. Liu, J. Zhai and J. Jia, *Nanoscale*, 2015, **7**, 11956–11961.
32 H. Wang, Y. Liang, Y. Li and H. Dai, *Angew. Chem., Int. Ed.*, 2011, **50**, 10969–10972.
33 D. Zhao, J.-L. Shui, L. R. Grabstanowicz, C. Chen, S. M. Commet, T. Xu, J. Lu and D.-J. Liu, *Adv. Mater.*, 2014, **26**, 1093–1097.
34 Y.-Z. Chen, C. Wang, Z.-Y. Wu, Y. Xiong, Q. Xu, S.-H. Yu and H.-L. Jiang, *Adv. Mater.*, 2015, **27**, 5010–5016.
35 C. W. Abney, J. C. Gilhula, K. Lu and W. Lin, *Adv. Mater.*, 2014, **26**, 7993–7997.
36 B. Chen, Z. Yang, Y. Zhu and Y. Xia, *J. Mater. Chem. A*, 2014, **2**, 16811–16831.

37 H.-L. Jiang, B. Liu, Y.-Q. Lan, K. Kuratani, T. Akita, H. Shioyama, F. Zong and Q. Xu, *J. Am. Chem. Soc.*, 2011, **133**, 11854–11857.
38 A. Aijaz, N. Fujiwara and Q. Xu, *J. Am. Chem. Soc.*, 2014, **136**, 6790–6793.
39 S. Ma, G. A. Goenaga, A. V. Call and D.-J. Liu, *Chem.–Eur. J.*, 2011, **17**, 2063–2067.
40 D. Zhao, J.-L. Shui, C. Chen, X. Chen, B. M. Reprogle, D. Wang and D.-J. Liu, *Chem. Sci.*, 2012, **3**, 3200–3205.
41 X. Wang, J. Zhou, H. Fu, W. Li, X. Fan, G. Xin, J. Zheng and X. Li, *J. Mater. Chem. A*, 2014, **2**, 14064–14070.
42 P. Su, H. Xiao, J. Zhao, Y. Yao, Z. Shao, C. Li and Q. Yang, *Chem. Sci.*, 2013, **4**, 2941–2946.
43 T. Palaniselvam, B. P. Biswal, R. Banerjee and S. Kurungot, *Chem.–Eur. J.*, 2013, **19**, 9335–9342.
44 Q. Li, P. Xu, W. Gao, S. Ma, G. Zhang, R. Cao, J. Cho, H.-L. Wang and G. Wu, *Adv. Mater.*, 2014, **26**, 1378–1386.
45 Y. Gong, H. Fei, X. Zou, W. Zhou, S. Yang, G. Ye, Z. Liu, Z. Peng, J. Lou, R. Vajtai, B. I. Yakobson, J. M. Tour and P. M. Ajayan, *Chem. Mater.*, 2015, **27**, 1181–1186.
46 Z. Jiang, W. Lu, Z. Li, K. H. Ho, X. Li, X. Jiao and D. Chen, *J. Mater. Chem. A*, 2014, **2**, 8603–8606.
47 W. Xia, J. Zhu, W. Guo, L. An, D. Xia and R. Zou, *J. Mater. Chem. A*, 2014, **2**, 11606–11613.
48 J. Tian, A. Morozan, M. T. Sougrati, M. Lefèvre, R. Chenitz, J.-P. Dodelet, D. Jones and F. Jaouen, *Angew. Chem., Int. Ed.*, 2013, **52**, 6867–6870.
49 Z. Yan, M. Cai and P. K. Shen, *J. Mater. Chem.*, 2012, **22**, 2133–2139.
50 J. Tang, T. Wang, X. Pan, X. Sun, X. Fan, Y. Guo, H. Xue and J. He, *J. Phys. Chem. C*, 2013, **117**, 16896–16906.
51 W. Ding, Z. Wei, S. Chen, X. Qi, T. Yang, J. Hu, D. Wang, L.-J. Wan, S. F. Alvi and L. Li, *Angew. Chem., Int. Ed.*, 2013, **52**, 11755–11759.
52 L. Lai, J. R. Potts, D. Zhan, L. Wang, C. K. Poh, C. Tang, H. Gong, Z. Shen, J. Lin and R. S. Ruoff, *Energy Environ. Sci.*, 2012, **5**, 7936.
53 Z. Luo, S. Lim, Z. Tian, J. Shang, L. Lai, B. MacDonald, C. Fu, Z. Shen, T. Yu and J. Lin, *J. Mater. Chem.*, 2011, **21**, 8038.
54 C. Battistoni, L. Gastaldi, G. Mattogno, M. G. Simeone and S. Viticoli, *Solid State Commun.*, 1987, **61**, 43–46.
55 S. Mao, Z. Wen, T. Huang, Y. Hou and J. Chen, *Energy Environ. Sci.*, 2014, **7**, 609–616.
56 F. Jaouen, E. Proietti, M. Lefèvre, R. Chenitz, J.-P. Dodelet, G. Wu, H. T. Chung, C. M. Johnston and P. Zelenay, *Energy Environ. Sci.*, 2010, **4**, 114–130.